CHAPTER 4

Studies of the methane steam reforming reaction at high pressure in a ceramic membrane reactor

4.1. Introduction

In this chapter, a membrane reactor study of the steam reforming of methane is presented. Methane steam reforming is an equilibrium-limited process involving three reversible reactions:

$$CH_4 + H_2O \rightleftarrows CO + 3H_2 \qquad \Delta H^0_{298} = 206\ kJ/mol \qquad (4.1)$$

$$CO + H_2O \rightleftarrows CO_2 + H_2 \qquad \Delta H^0_{298} = -41\ kJ/mol \qquad (4.2)$$

$$CH_4 + 2H_2O \rightleftarrows CO_2 + 4H_2 \qquad \Delta H^0_{298} = 165\ kJ/mol \qquad (4.3)$$

The studies used a novel silica-alumina membrane prepared by using the chemical vapor deposition (CVD) technique as mentioned in detail in Chapter 1. The conversion of methane, consumption rates of the reactants and the products yields obtained in a packed-bed reactor (PBR) were compared to those of a membrane reactor (MR) at various temperatures (773-923 K) and pressures (1-20 atm) using a commercial $Ni/MgAl_2O_4$ catalyst. The conversion of methane was improved significantly in the MR by the countercurrent removal of hydrogen at all temperatures and allowed product yields higher

than equilibrium to be obtained. Pressure had a positive effect on the hydrogen yield because of the increase in driving force for the permeance of hydrogen.

4.2. Experimental

4.2.1. Catalyst preparation and characterization

A commercial $Ni/MgAl_2O_4$ catalyst (NG-610-6H) provided by Unicat Catalysts was used throughout the study. The original catalyst was crushed and sieved to sizes of 0.1-0.3 mm. A quantity of 2 g of this catalyst was mixed with 1 g of inert quartz chips of the same size to make up a catalyst bed of 5 cm length to match the length of the membrane zone. The catalyst was reduced in hydrogen at 923 K for 2 h before use.

The BET surface area was obtained from the nitrogen adsorption isotherm carried out in a volumetric adsorption unit (Micromeritics, ASAP 2010). The catalyst sample was degassed at 393 K in vacuum prior to the measurements. The CO uptake of the catalyst was determined after reduction in 75 μmol s^{-1} (110 cm^3 (NTP) min^{-1}) of hydrogen at 823 K for 2 h in a flow system. Pulses of CO were injected into a He carrier stream at room temperature and the intensity of the CO signal (m/e = 28) was monitored with a mass spectrometer (Dycor/Ametek Model MA100). The injection of CO was continued until saturation of the sample surface was observed.

4.2.2. Preparation of hydrogen selective silica-alumina membranes

Hydrogen selective silica-alumina membranes similar to those reported in Chapter 1 were used in these studies. They were prepared by chemical vapor deposition (CVD) of a thin permselective layer on a porous alumina support at 923 K. The support was a commercial multilayered porous alumina support (Pall Corporation Part No. S700-0011) of tubular geometry (OD=10 mm, ID=7 mm) with a 5 nm outer pore size. A length of 5 cm of this support was connected to dense alumina tubing at both ends by thermal treatment of a glass glaze (Duncan, IN, Part No. 1001) at 1153 K. The inside of the membrane was then dip-coated in a 0.05 M dispersion of boehmite sol for 10 s and dried at room temperature for 24 h. After drying, the membrane was calcined at 973 K for 2 h and at 923 K for 6 h.

4.2.3. Steam reforming of methane with a membrane reactor

The steam reforming of methane was conducted at various temperatures (773, 798, 823, 848, 873, 898, 923 K) and pressures (1, 5, 10, 15, 20 atm) in a packed-bed reactor (PBR) and in a membrane reactor (MR). A mixture of steam and methane (S/C = 3/1) was fed continuously to the reactor at a methane flow rate of 3.35 μmol/s (5.0 cm^3 (NTP) min^{-1}) at atmospheric conditions. While the ratio of steam to methane was kept at 3 to 1, the overall inlet flow rate of the reactants was increased proportionally to the pressure to keep the residence time constant. The flow rates are tabulated in Table 4.1.

Table 4.1 Inlet flows of reactants

Pressure (atm)	Volumetric flowrate of CH_4 (cm^3 (NTP) min^{-1})	Volumetric flowrate of H_2O (cm^3 (NTP) min^{-1})
1	5	15
5	25	75
10	50	150
15	75	225
20	100	300

The reactor was specifically designed to operate at high pressure. It comprised three concentric tubular sections which consisted of a stainless steel outer shell, a quartz liner and the membrane tube. The sections were assembled concentrically with O-rings as shown in Figure 1. The annular section between the quartz liner and the membrane held the catalyst and was denoted as the shell side of the reactor. The innermost membrane section was denoted as the tube side of the reactor. The shell feed line was split into two inlet lines which were connected to the upper part of the stainless steel shell. One of the inlet lines fed the section between the quartz liner and membrane while the other one was connected to the thin section between the stainless steel shell and quartz liner. There was no flow in this section, and the connection was simply used to equalize the pressure on both sides of the quartz liner. The products left the reactor from the shell side where the reaction took place. A back pressure regulator at the exit allowed the pressure to be increased simultaneously on both sides of the quartz sleeve. A separate back pressure regulator was used to control the pressure on the tube side. For the experiments described in this paper the pressure in the tube side was maintained at 1 atm. The direct contact of

the catalyst with the stainless steel outer shell was avoided by this configuration which was important as previous studies had found the stainless steel to promote carbon formation [1]. The tube side inlet line was connected to the membrane on the bottom side of the reactor and permitted the permeated gases to be swept away from the top side of the reactor to provide the benefits of countercurrent flow. An impermeable quartz tube was used instead of the membrane for the studies in the packed-bed reactor configuration to keep the geometry the same.

The catalyst pellets diluted with quartz chips of the same size was loaded in the section between the quartz liner and membrane along the silica-alumina membrane zone. The bed was supported with quartz wool and was preceded by a bed of the inert quartz chips to provide better heating and mixing of the reactants. The reactor was installed in an electric furnace and the temperature was increased at a ramping rate of 0.016 K s^{-1} (1 K min^{-1}) to the reaction temperature with respective argon flows of 33.5 μmol s^{-1} (50 cm^3 (NTP) min^{-1}) and 67 μmol s^{-1} (100 cm^3 (NTP) min^{-1}) through the shell and tube side of the reactor before the introduction of hydrogen at a flow rate of 33.5 μmol s^{-1} (50 cm^3 (NTP) min^{-1}) for 2 h on the shell side to reduce the catalyst. After the reduction, the reactants (CH_4 and H_2O) were fed to the shell side of the reactor while the argon flow was continued to be used as sweep gas through the tube side of the reactor. The back pressure regulators were used to adjust the pressures on the shell and tube sides of the reactor. Both of the streams passed through a condenser unit to remove moisture before injection into an on-line gas chromatograph (SRI 8610). The compositions of the streams (H_2, CH_4, CO, CO_2) were determined by an on-line gas chromatograph using a carbosphere packed column

(OD: 3.175 mm, L: 1.900×10^3 mm) attached to a thermal conductivity detector. The total volumetric flow rates of the shell and tube sides were measured by a bubble flow meter.

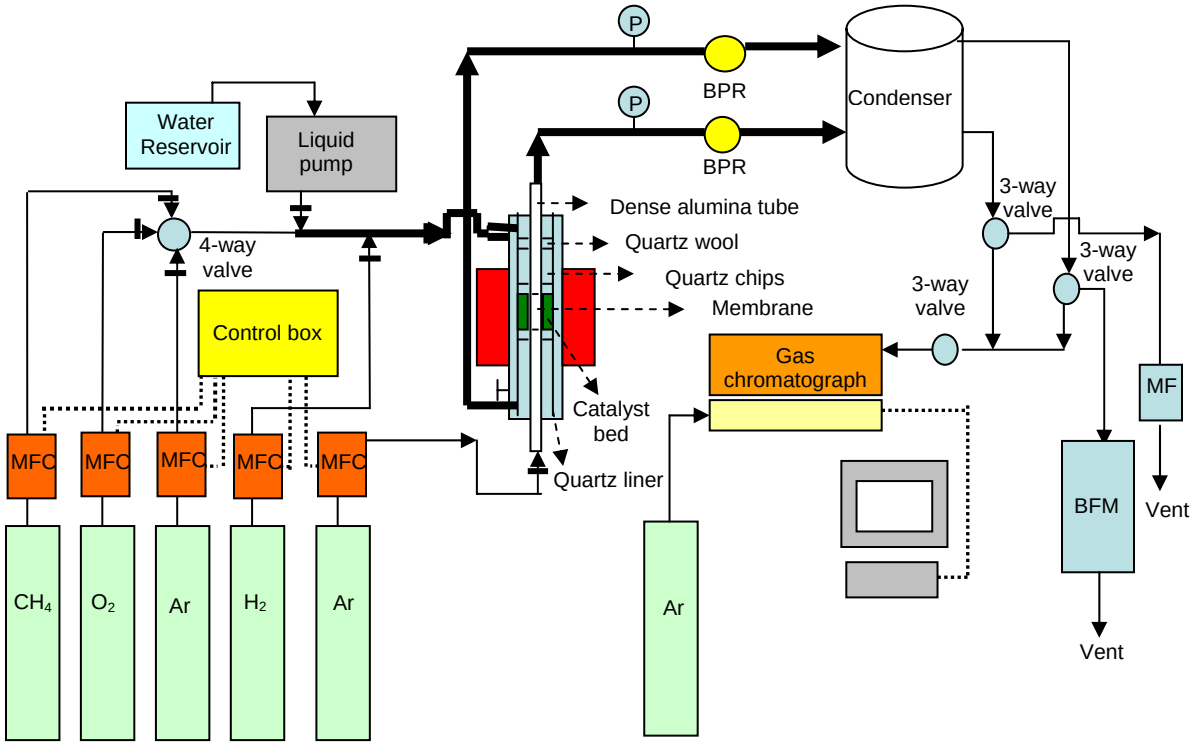

Figure 4.1. Schematic diagram of the reactor system

The conversion and utilization of the reactants were calculated according to the following equations,

$$Conversion(i) = \left(\frac{F_i^{in} - F_i^{out}}{F_i^{in}} \right) \tag{4.4}$$

$$Utilization(i) = \left(\frac{F_i^{in} - F_i^{out}}{m} \right) \quad (4.5)$$

$$Yield(j) = \left(\frac{F_j^{out}}{m} \right) \quad (4.6)$$

where F_i^{in} is the inlet flow rate (mol s^{-1}) of reactant species i, F_i^{out} is the outlet flow rate (mol s^{-1}) of unreacted species i measured at the end of the reactor, F_j^{out} is the outlet flow rate (mol s^{-1}) of produced species j measured at the end of the reactor and m is weight of the catalyst. The sum of the flow rates of reactant species in the shell and tube side were used to calculate the conversion, the utilization of the reactants and the yield of the products in the membrane reactor.

4.3. Results and Discussion

4.3.1. Catalyst properties and membrane performances

The BET surface area and the CO uptake of the commercial $Ni/MgAl_2O_4$ catalyst were measured to be 150 m^2 g^{-1} and 275 μmol g^{-1} respectively.

In this study, the alumina-silica membranes were utilized at a point where they were stable after showing about 60 % loss of their initial hydrogen permeability. The permeance of hydrogen at different pressures was also measured and are presented in Figure 4.2. A

linear relationship was found between the flux of hydrogen through the membrane and the pressure, confirming that the mechanism of permeation is molecular.

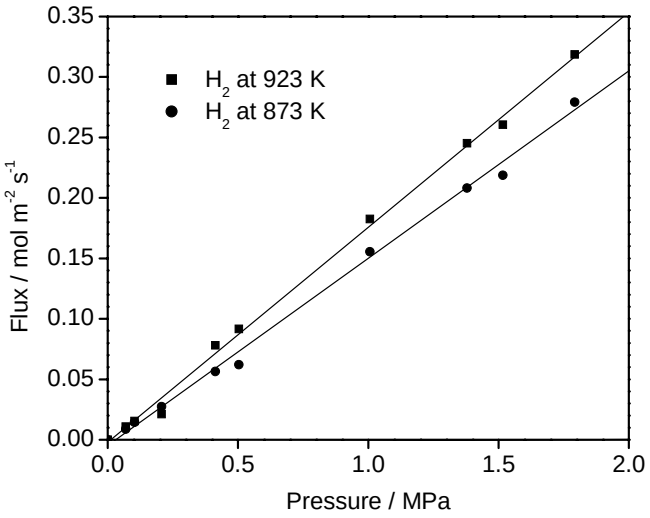

Figure 4. 2. Flux of hydrogen through the silica-based membrane versus pressure

4.3.2. Effect of temperature on the performances of the MR and the PBR

The effect of temperature on the conversion of methane at 1 atm in the membrane reactor and the packed-bed reactor is shown in Figure 4.3a). The conversion values of the PBR closely matched the values obtained from equilibrium calculations (dotted lines) at all temperatures. The following equilibrium equations can be written for the steam reforming and water-gas shift reactions, where P is the pressure and the y's are mole fractions.

$$K_1 = \frac{y_{CO} y_{H_2}^3}{y_{CH_4} y_{H_2O}} P^2 \qquad (4.7)$$

$$K_2 = \frac{y_{CO_2} y_{H_2}}{y_{CO} y_{H_2O}} \tag{4.8}$$

The equilibrium methane conversions were calculated by solving these equations simultaneously with values for K_1 and K_2 obtained at different temperatures from Chemeq which is a basic language program for the calculation of the standard state heat and free energy of reactions and the chemical equilibrium constants [2]. For the membrane reactor the effect of hydrogen removal is clearly observable as the methane conversions increase to higher values at all temperatures. In the PBR the fractional methane conversions were 0.44 and 0.90 at 773 and 923 K respectively while they reached values of 0.56 and 0.97 at the same temperatures in the MR.

The utilizations of CH_4 and H_2O in the PBR and the MR in the same temperature range are shown in Figure 4.3b). The equilibrium utilizations were also calculated from the equilibrium conversions and the inlet flow rates of the reactants and were normalized by the catalyst weight. A nonlinear trend was observed for the utilizations of CH_4 and H_2O both in the PBR and MR, and a slightly higher level-off point was observed in the MR at higher temperatures.

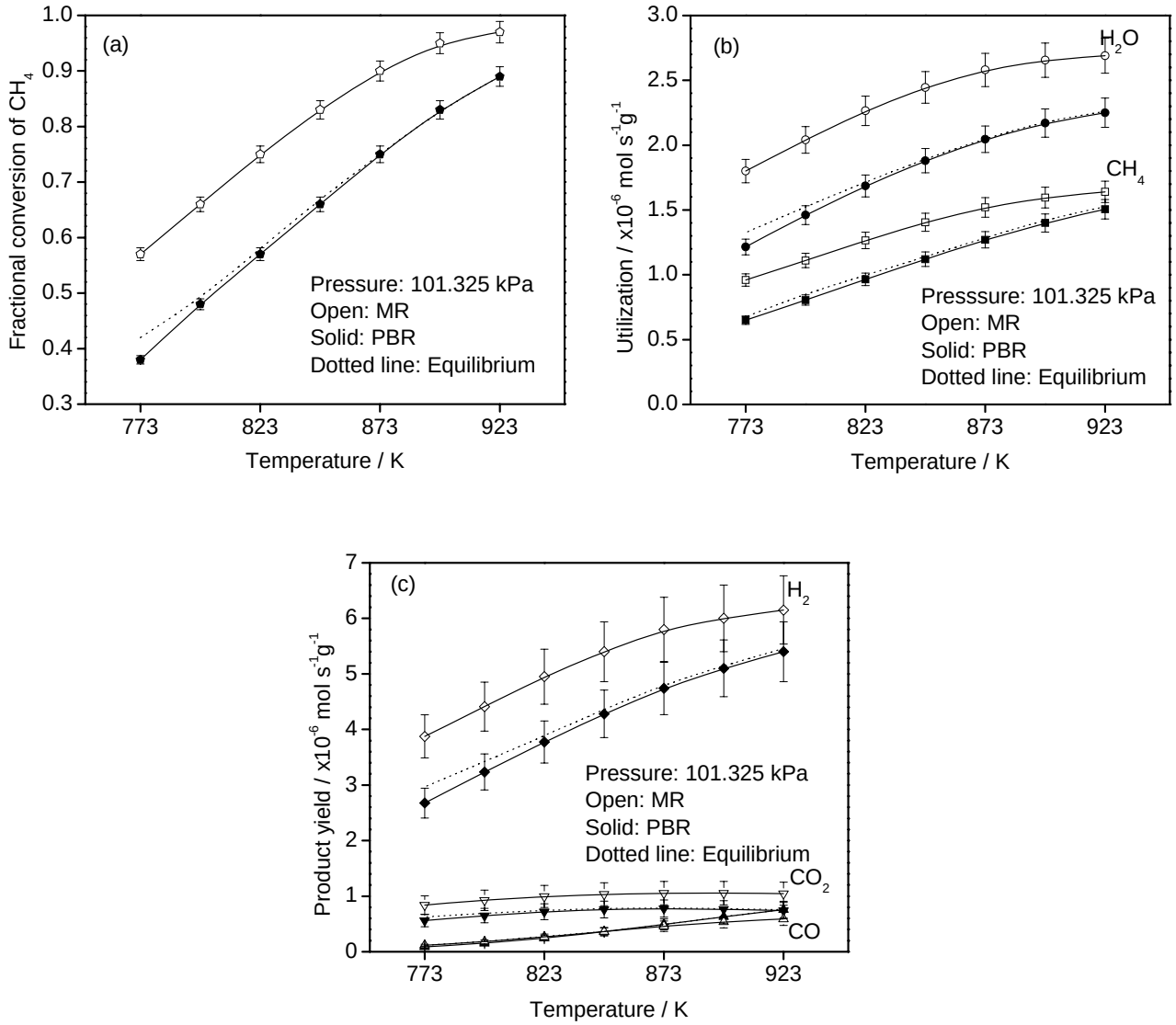

Figure 4.3 a) Fractional conversion of CH_4 in the PBR and the MR at atmospheric pressure, b) Utilization of CH_4 and H_2O in the PBR and the MR at atmospheric pressure, c) Yield of H_2, CO and CO_2 in the PBR and the MR at atmospheric pressure

The yields of H_2, CO and CO_2 in the packed-bed and the membrane reactor are presented in Figure 4.3c). The yields in the membrane reactor are the sum of the yields in

the permeate and the retentate sides. In the packed bed reactor, the H_2 and CO yields increased while the CO_2 yields reached a plateau with increasing temperature. A similar trend was observed in the MR with higher product yields except for that of CO at all temperatures. The CO yields were comparable both in the PBR and the MR at lower temperatures but the production of CO was favored by the PBR at and above 873 K.

4.3.2. Effect of pressure on the performances of the MR and the PBR

The effect of pressure on the steam reforming of methane at 873 K is presented in Figure 4. The equilibrium methane conversions and the experimental conversions in the PBR and the MR had a similar decreasing trend with increasing pressure as seen in Figure 4.4 a). As mentioned in the previous section, the steam reforming reaction is not favored thermodynamically at high pressure due to the net increase of moles on the product side. The methane conversions in the PBR were slightly lower than the equilibrium values notably at higher pressures. In the MR the enhancing effect of separation through the membrane on the methane conversion was clearly observed with much higher conversion values attained at all pressures. However, the permeance of hydrogen was not high enough to overcome the effect of thermodynamics due to the increase in moles in the reaction, and the methane conversion decreased with increasing pressure. The enhancement in the methane conversion is defined as $X_{CH_4}(MR) / X_{CH_4}(PBR) \times 100$ and is presented in Figure 4.4 b). The CH_4 conversion enhancement increased with increasing pressure and at 20 atm reached a value of 190 % the value obtained in the PBR.

The utilizations of CH_4 and H_2O in the PBR and the MR at 873 K are presented in Figure 4.4 c). In the PBR the utilizations of both CH_4 and H_2O increased with pressure, a trend also observed in the MR. The trends in the utilizations in the PBR and the MR were somewhat different at the lowest and the highest pressures. In the MR there was a constant increase in the utilization values while the values leveled-off with increasing pressures in the PBR. The utilizations of CH_4 and H_2O in the PBR (CH_4: 1.25×10^{-6} mol s^{-1} g^{-1}, H_2O: 2.0×10^{-6} mol s^{-1} g^{-1}) were lower than the utilizations observed in the MR (CH_4: 1.5×10^{-6} mol s^{-1} g^{-1}, H_2O: 2.55×10^{-6} mol s^{-1} g^{-1}) at atmospheric conditions. At 2026.5 kPa the utilizations of CH_4 and H_2O in the MR (CH_4: 15×10^{-6} mol s^{-1} g^{-1}, H_2O: 25.5×10^{-6} mol s^{-1} g^{-1}) were significantly higher than the equilibrium values and those in the PBR (CH_4: 7.45×10^{-6} mol s^{-1} g^{-1}, H_2O: 14×10^{-6} mol s^{-1} g^{-1}).

The yields of H_2, CO and CO_2 in the PBR were below the equilibrium values at all pressures as seen in Figure 4.4 d). The yield of CO in the MR was just above the equilibrium value and that in the PBR while the yield of CO_2 in the MR was higher than that in the PBR at higher pressures. There is an increasing trend with pressure for the H_2 yield and much higher yields were obtained in the MR than in the PBR at all pressures. The values were also above the equilibrium values.

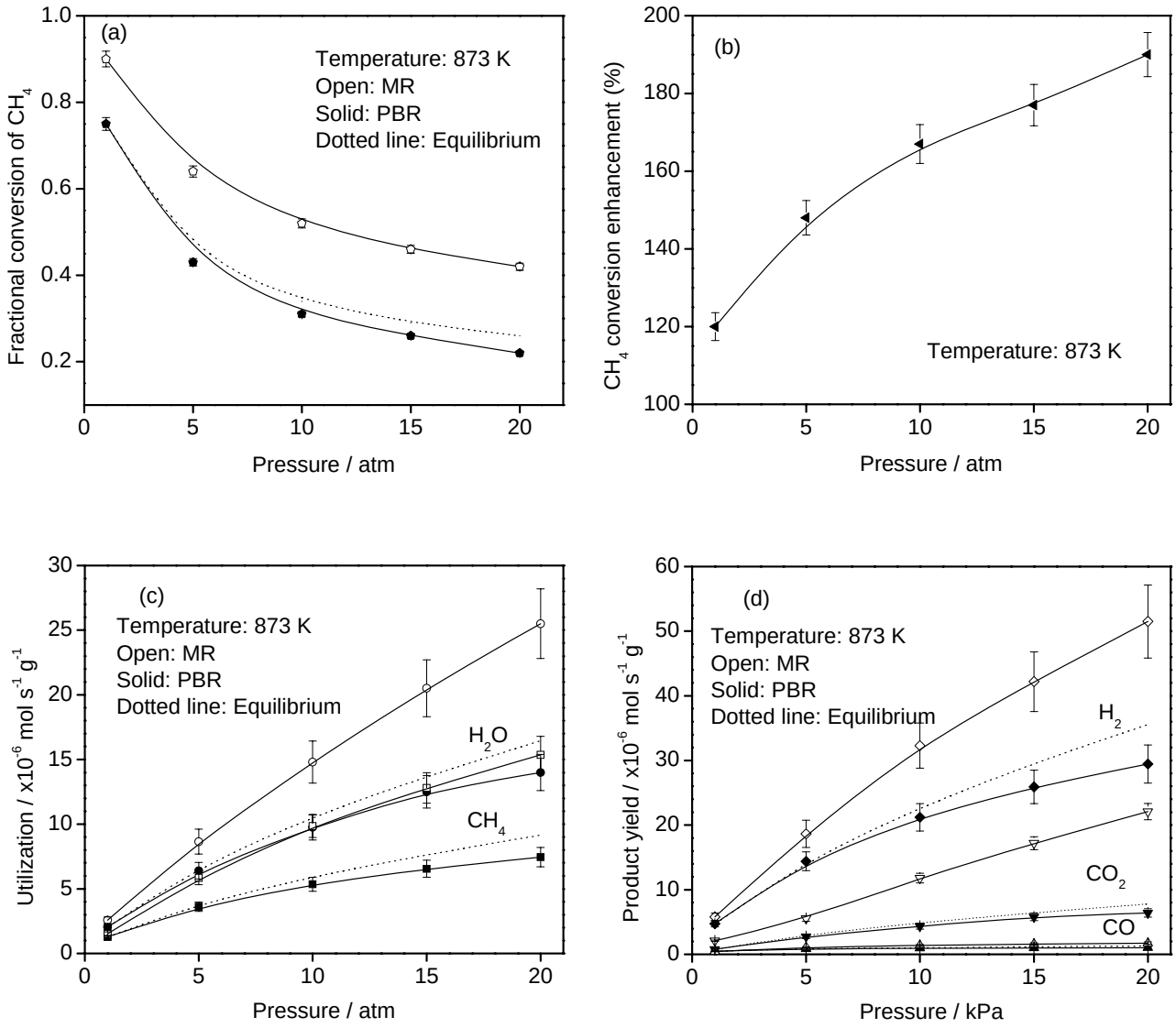

Figure 4.4 a) Fractional conversion of CH_4 in the PBR and the MR at 873 K, b) Enhancement in the CH_4 conversion in the PBR and the MR at 873, c) Utilization of CH_4 and H_2O in the PBR and the MR at 873 K, d) Yield of H_2, CO and CO_2 in the PBR and the MR at 873 K

The conversion of methane both in the PBR and the MR increased considerably with increase in the temperature from 873 K to 923 K (Figure 4.5 a). Equilibrium conditions for the steam reforming reaction were still maintained at 923 K in the PBR. At higher pressures (15 and 20 atm), there is a little deviation from equilibrium at 873 K and 923 K. Similarly, the conversion of methane in the MR was higher than the conversion in the PBR at atmospheric conditions. At 2026.5 kPa much higher enhancement in the methane conversion was observed than at atmospheric conditions and this enhancement was significant at 923 K as clearly seen in Figure 4.5 b). The CH_4 conversion enhancement again showed an increasing trend with increasing pressure and reached a value of 180 % at 923 K

The utilizations of CH_4 and H_2O in the PBR and the MR at 923 K are also shown in Figure 4.5 c). The trends of utilizations for the PBR and the MR at 923 K were similar to those at lower temperature. The enhancement in the utilization of H_2O was again much higher than the enhancement in the utilization of CH_4 for the MR. The increase in temperature resulted in much higher utilization values especially at higher pressures. The utilizations of CH_4 and H_2O in the MR (CH_4: 1.6×10^{-6} mol s^{-1} g^{-1}, H_2O: 2.65×10^{-6} mol s^{-1} g^{-1}) were significantly higher than those in the PBR (CH_4: 1.5×10^{-6} mol s^{-1} g^{-1}, H_2O: 2.25×10^{-6} mol s^{-1} g^{-1}) at atmospheric conditions. At 20 atm the utilizations of CH_4 and H_2O in the MR (CH_4: 19.5×10^{-6} mol s^{-1} g^{-1}, H_2O: 34.5×10^{-6} mol s^{-1} g^{-1}) were significantly higher than those in the PBR (CH_4: 10.4×10^{-6} mol s^{-1} g^{-1}, H_2O: 19.0×10^{-6} mol s^{-1} g^{-1}).

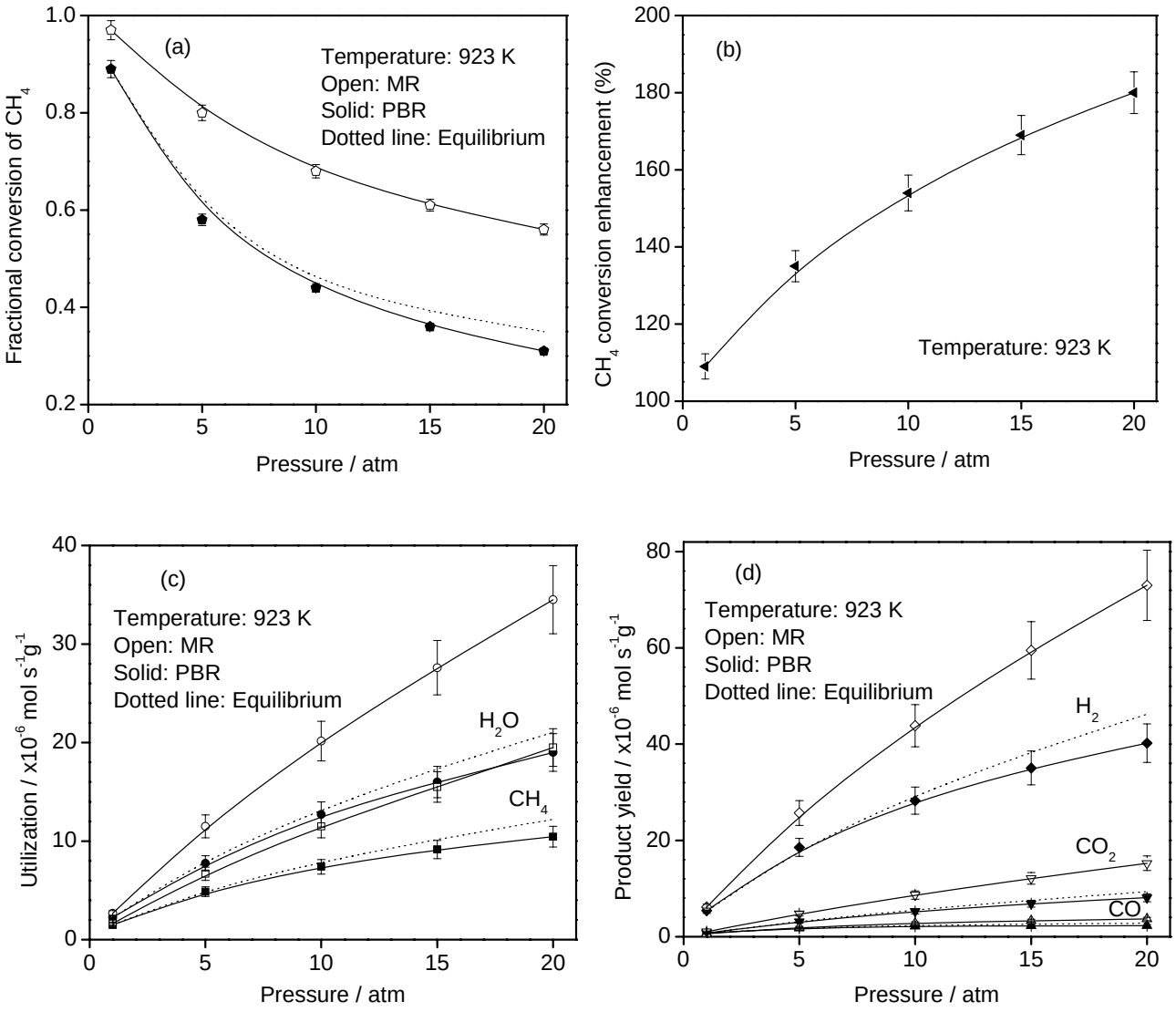

Figure 4.5 a) Fractional conversion of CH_4 in the PBR and the MR at 923 K, b) Enhancement in the CH_4 conversion in the PBR and the MR at 923 K, c) Utilization of CH_4 and H_2O in the PBR and the MR at 923 K, d) Yield of H_2, CO and CO_2 in the PBR and the MR at 923 K

The yields of CO and CO_2 were close to the equilibrium values at lower pressures and just below the equilibrium values at higher pressures as seen in Figure 4.5 d). The only

exception was the H_2 yield which was much lower than the equilibrium values in the PBR above atmospheric pressure. There was an increasing trend with pressure for the H_2 yield and much higher yields were obtained in the MR than in the PBR at all pressures. At 2026.5 kPa the yields of H_2, CO and CO_2 in the MR (H_2: 73.0×10^{-6} mol s^{-1} g^{-1}, CO: 3.65×10^{-6} mol s^{-1} g^{-1}, CO_2: 15.2×10^{-6} mol s^{-1} g^{-1}) were also higher than those in the PBR (H_2: 40.2×10^{-6} mol s^{-1} g^{-1}, CO: 2.3×10^{-6} mol s^{-1} g^{-1}, CO_2: 8.1×10^{-6} mol s^{-1} g^{-1}) at a higher temperature.

A comparison with some experimental results published in the literature was made and the performances of various membranes and the operating conditions of the corresponding membrane reactor applications are summarized in Table 4.2. In Table 4.2, the first five rows describe results obtained with palladium membranes and the last five rows describe results obtained with various types of silica and alumina membranes. When the performances of the membranes are compared, the palladium membranes are seen to have significantly higher permeances than the silica and alumina membranes. The units of the permeance of palladium membranes (cm^3 cm^{-2} min^{-1} $atm^{-0.5}$) are converted into SI units of the permeance (mol m^{-2} s^{-1} Pa^{-1}) using the inlet and outlet pressures for easy comparison. The catalysts were dispersed in the alumina membranes whereas they were sandwiched between the alumina support and the layers of silica for the microporous membranes. The conversion of methane fell in the range of 60 to 90% at various space velocities for all membrane reactors and the equilibrium conversion of methane was equal to 44 % at 773 K and 1 atm. Comparison of CH_4 conversions and H_2 yields obtained in the membrane reactor are compared to equilibrium values in the last two columns. The use of membrane

reactors produced significant enhancements in these quantities in all cases. The membrane prepared in this study had a permeance of 1.0×10^{-7} mol m^{-2} s^{-1} Pa^{-1} in its fresh state, and this became 4.0×10^{-8} mol m^{-2} s^{-1} Pa^{-1} after exposure to steam and during use, a 60 % drop. The conversion of methane reached a value of 57 % at a space velocity of 700 h^{-1} versus 44 % at equilibrium at 101.325 kPa and 56 % versus 85 % at 20 atm. From this comparison, it is concluded that higher permeance membranes should be used to obtain better conversions of methane and higher yields of hydrogen. The significance of the results with the silica-based membrane of this study is demonstration of its applicability at higher temperatures (873 K and 923 K) and at higher pressures (15 and 20 atm) which is important for practical applications.

Table 4.2. Performance of methane steam reforming processes with membrane reactors

Membrane type	Membrane properties and performances	SMR conditions	CH_4 conversions eq→exp (%)	H_2 yields eq→exp ($\times 10^{-6}$ mol s^{-1} g^{-1})
Pd-PG [3]	ELP, 20 μm $P=1.2\times10^{-6}$ mol m^{-2} s^{-1} Pa^{-1}	T=773 K, P=0.1 MPa, S/C=3 Ni/Al_2O_3 13g, CH4=25cm^3min^{-1} SV 115$cm^3g^{-1}h^{-1}$	44→88	2.51→5.03
		T=773 K, P=0.9 MPa, S/C=3 Ni/Al_2O_3 13g, CH4=75cm^3min^{-1} SV 346$cm^3g^{-1}h^{-1}$	21→92	3.60→15.7
Pd-MPSS [4]	ELP, 19.8 μm $P=1.4\times10^{-6}$ mol m^{-2} s^{-1} Pa^{-1}	T=773 K, P=0.13 MPa, S/C=3 Ni/Al_2O_3 11g, CH4=40cm^3min^{-1} SV 218 $cm^3g^{-1}h^{-1}$	44→63	4.76→6.81
Pd-MPSS [5]	ELP, 6 μm $P=2.9\times10^{-6}$ mol m^{-2} s^{-1} Pa^{-1}	T=773 K, P=300kPa, S/C=3 Ni/Al_2O_3 15g, CH4=25cm^3min^{-1} SV 100$cm^3g^{-1}h^{-1}$	44→98	2.18→4.86
Pd-Ag [6]	ELP, 5.8 μm $P=2.7\times10^{-6}$ mol m^{-2} s^{-1} Pa^{-1}	T=773 K, P=0.1 MPa, S/C=3 Ni 6.5g, SV 692$cm^3g^{-1}h^{-1}$	44→80	15.1→27.4
Pd-Ag [7]	Cold rolling, 50 μm $P=2.2\times10^{-6}$ mol m^{-2} s^{-1} Pa^{-1}	T=723 K, P=0.12 MPa, S/C=3 Ni/Al_2O_3 3.1g, CH4=7.3cm^3min^{-1} SV 141 $cm^3g^{-1}h^{-1}$	27→50	1.89→3.50
MsP-Al [8]	Rh dispersed $P=1.7\times10^{-7}$ mol m^{-2} s^{-1} Pa^{-1}	T=773 K, P=0.12 MPa, S/C=3 Ru/Al_2O_3, SV 750 h^{-1}	44→85	1.76→3.4*

McP-Si [9]	Sandwich-type $P=2.6\times10^{-7}$ mol m^{-2} s^{-1} Pa^{-1}	T=773 K, P=0.1 MPa, S/C=3 Ni/Al_2O_3, SV 483-1612$cm^3g^{-1}h^{-1}$	44→80-58	10.5→19.1-45.9
McP-Si-Zr [10]	Sandwich-type $P=3.4\times10^{-6}$ mol m^{-2} s^{-1} Pa^{-1}	T=773 K, P=0.1 MPa, S/C=5 Ni 0.25 g, CH4=2.4 cm^3min^{-1} SV 576 $cm^3g^{-1}h^{-1}$	59→33	4.21→2.55
		T=773 K, P=0.6 MPa, S/C=5 Ni 0.25 g, CH4=2.4 cm^3min^{-1} SV 576 $cm^3g^{-1}h^{-1}$	31→49	8.8→14.0
McP-Al [11]	Ru dispersed $P=1.3\times10^{-7}$ mol m^{-2} s^{-1} Pa^{-1}	T=748 K, P=0.1 MPa, S/C=3 Ru/Al_2O_3, SV 750 h^{-1}	40→80	1.76→3.28*
Al-Si (this work)	$P=6.0\times10^{-8}$ mol m^{-2} s^{-1} Pa^{-1}	T=773 K, P=0.1 MPa, S/C=3 $Ni/MgAl_2O_4$ 2 g, CH4=4.5 cm^3min^{-1} SV 135 $cm^3g^{-1}h^{-1}$	44→57	2.94→3.81
		T=923 K, P=2 MPa, S/C=3 $Ni/MgAl_2O_4$ 2 g, CH4=90 cm^3min^{-1} SV 2700 $cm^3g^{-1}h^{-1}$	35→56	46.2→73.0

PG, porous glass; MPSS, macro porous stainless steel; MsP, mesoporous; McP, micro porous; ELP, electroless plating; S/C, steam to methane ratio

* $Y_{H_2} = 4 \times X_{CH_4}$ which Y_{H_2} is hydrogen yield and X_{CH_4} is methane conversion; Eq. Equilibrium value;

Exp, Experimental value obtained in the membrane reactor

4.4. Conclusions

The steam reforming of methane was studied experimentally in a packed-bed reactor (PBR) and a membrane reactor (MR) at various temperatures (773-923 K) and pressures (1-20 atm). The silica-based membrane used in the MR was moderately hydrogen permeable and hydrothermally stable. A similar geometry was used in both the PBR and MR except that the PBR employed a non-permeable quartz tube instead of the membrane tube. A commercial $Ni/MgAl_2O_4$ catalyst was used in both of the reaction systems. The conversions of methane obtained from the PBR at various temperatures showed that the steam reforming of methane operated at equilibrium. In the MR higher conversions were obtained due to the removal of hydrogen from the system, which shifted the equilibrium in the forward direction.

The effect of pressure on the steam reforming of methane was also investigated in the PBR and the MR. The steam reforming of methane is not favored at higher pressures because of the increase in moles in the reaction. However, permeance increased at higher pressures because of the increase in driving force. Significant enhancements were obtained with the MR over the PBR at higher pressures.

This study also compares the results of the membrane reactor studies found in the literature at 773 K. This temperature was chosen for comparison because data for palladium membrane is restricted to this maximum temperature. The conversion of methane and the hydrogen yield obtained in this study are in the range obtained in the literature. Much higher H_2

yields at higher pressures indicate that the amount of hydrogen removal has a significant effect on the performance of the steam reforming reaction.

References

[1] D.Lee, Studies on hydrogen selective silica membranes and the catalytic reforming of CH_4 with CO_2 in a membrane reactor, VPI&SU University Libraries, 2003

[2] S. I. Sandler, Chemical and Engineering Thermodynamics. 3rd ed. John Wiley and Sons, 1999, A9.1

[3] S. Uemiya, N. Sato, H. Ando, T. Matsuda, E. Kikuchi, Appl Catal, 67 (1991) 223

[4] J. Shu, B. P. A. Grandjean, S. Kaliaguine, Appl. Catal. A, 119 (1994) 305

[5] Tong, Y. Matsumura, H. Suda, K. Haraya, Ind. Eng. Chem. Res. 44 (2005) 1454

[6] E. Kikuchi, S. Uemiya, T. Matsuda, Stud. Surf. Sci. Catal. 61 (1991) 509

[7] F. Gallucci, L. Paturzo, A. Fama, A. Basile, Ind. Eng. Chem. Res. 43 (2004) 928

[8] M. Chai, M. Machida, K. Eguchi, H. Arai, Appl. Catal. A. 110 (1994) 239

[9] T. Tsuru, K. Yamaguchi, T. Yoshioka, M. Asaeda. AIChE J. 50 (2004) 2794

[10] T. Tsuru, T. Tsuge, S. Kubota, K. Yoshida, T. Yoshioka, M. Asaeda, Sep. Sci. Technol., 36 (2001) 3721

[11] K. Eguchi, M. R. Chai, M. Machida, H. M. Arai. Sci. Tech. in Catal., 37 (1994) 251